PAPER • OPEN ACCESS

Nanoscale insights into the structure of solution-processed graphene by x-ray scattering

To cite this article: Zhengyu Yan *et al* 2023 *2D Mater.* **10** 015006

View the article online for updates and enhancements.

2D Materials

PAPER

Nanoscale insights into the structure of solution-processed graphene by x-ray scattering

Zhengyu Yan[1], María J G Guimarey[2,3], Khaled Parvez[4], Chaochao Dun[5], Oliver Read[4], Thomas Forrest[6], Jeffrey J Urban[5], Amor Abdelkader[2], Cinzia Casiraghi[4] and Wajira Mirihanage[1,*]

[1] Department of Materials, The University of Manchester, Manchester, M13 9PL, United Kingdom
[2] Department of Engineering, Bournemouth University, Poole BH12 5BB, United Kingdom
[3] Nafomat Group, Department of Applied Physics, University of Santiago de Compostela, 15782 Santiago de Compostela, Spain
[4] Department of Chemistry, The University of Manchester, Manchester, M13 9PL, United Kingdom
[5] The Molecular Foundry, Lawrence Berkeley National Laboratory, Berkley, CA 94720, United States of America
[6] Diamond Light Source, Didcot, OX11 0DE, United Kingdom
[*] Author to whom any correspondence should be addressed.

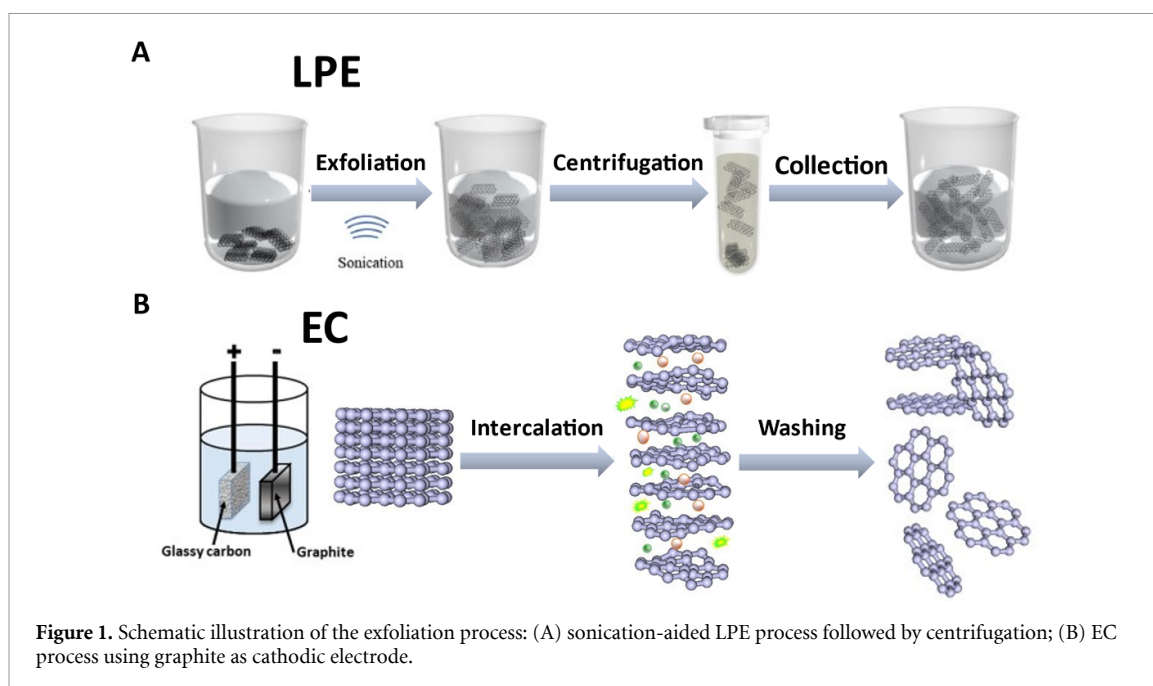**E-mail:** wajira.mirihanage@manchester.ac.uk

Abstract

Chemical exfoliation is an attractive approach for the synthesis of graphene due to its low cost and simplicity. However, challenges still remain in the characterization of solution-processed graphene, in particular with atomic resolution. Through this work we demonstrate the x-ray pair distribution function as a novel approach to study solution-processed graphene or other 2D materials with atomic resolution, directly in solution, produced by liquid-phase and electrochemical exfoliations. The results show the disappearance of long-range atomic correlations, in both cases, confirming the production of single and few-layer graphene. In addition, a considerable ring distortion has been observed as compared to graphite, irrespective of the solvent used: the normal surface angle to the sheet of the powder sample should be less than 6°, compatible with ripples formation observed in suspended graphene. We attribute this effect to the interaction of solvent molecules with the graphene nanosheets.

1. Introduction

One of the most attractive and industrially scalable methods for graphene production is given by chemical exfoliation of graphite [1–4]. This approach gives rise to graphene dispersions, which can be further processed with simple and low-cost methods such as drop casting and inkjet printing [5–8]. The most used chemical exfoliation approaches are liquid phase exfoliation (LPE) and electrochemical exfoliation (EC). The LPE method relies on the use of ultrasound and/or shear force to exfoliate bulk graphite into graphene suspended in a suitable solvent, such as N-Methyl-2-pyrrolidone (NMP), N,N-dimethylformamide (DMF), and Cyrene (Cy) [9–11]. The EC process is based on expanding the graphite layers following the intercalation of ions and small molecules driven by an external electric field. According to the charge of

the intercalated ions, the graphite electrode works as an anode or cathode, hosting oxidation or reduction reactions, respectively [12–14]. Cathodic EC gives rise to defect-free graphene, but exfoliation does require several hours [15, 16], while anodic EC is quick but gives rise to slightly oxidised graphene [14].

Despite the use of simple methods to produce solution-processed graphene, its characterisation is very challenging because the nanosheets come in different sizes, thicknesses and chemical functionalisation [10]. In addition, the lack of metrology standards strongly limits the commercialisation of graphene-based products [10, 17, 18]. Only recently, the community has defined some guidelines for the characterisation of graphene-based materials [19], which led to the development of the first ISO/IEC standard (ISO/TS 21356-1:2021) for measuring the structural properties of graphene [20]. In particular, information on the atomic

Figure 1. Schematic illustration of the exfoliation process: (A) sonication-aided LPE process followed by centrifugation; (B) EC process using graphite as cathodic electrode.

structure of solution-processed graphene is currently provided by transmission electron microscopy, which requires specific sample preparation, and it is time-consuming, so it can only be performed on a selected number of nanosheets. The electron beam can also damage or change the structure of the nanosheets.
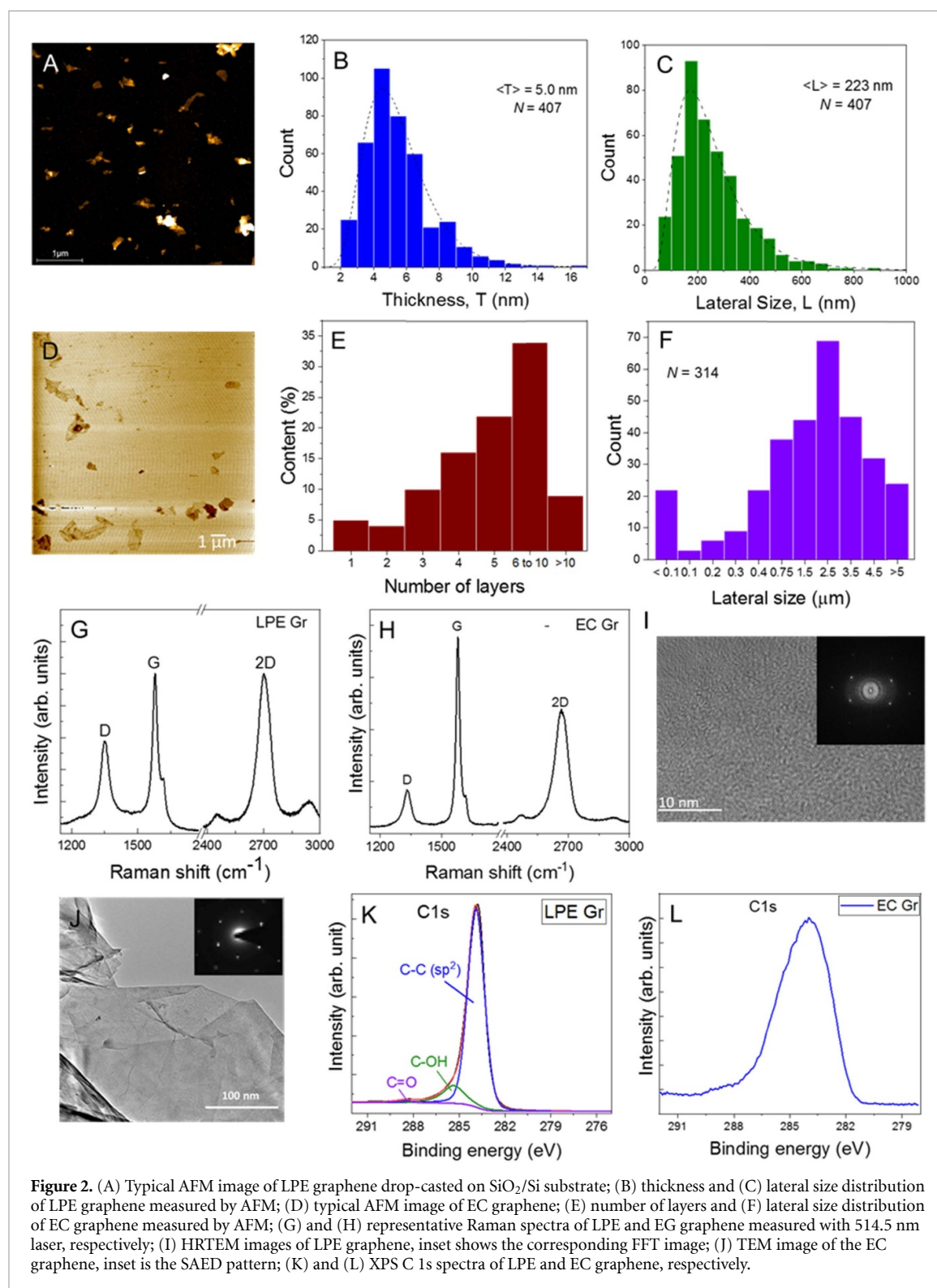
Synchrotron x-ray based characterisation techniques are increasingly employed in material science [21–24] because of their high photon energy (shorter wavelengths), increased penetration, and short measuring time due to the appreciable photon flux, hence providing an elegant solution for materials characterisation. In particular, the x-ray pair distribution function (XPDF) [24] can provide quantitative information on the crystal structure, e.g. the average distances between the neighbouring atoms, enabling insights into the material structure with nanoscale resolution. Nevertheless, to the best of our knowledge, these types of measurements have been rarely performed on graphene-based materials. Previous studies with high energy x-rays [25–28] focussed on the study of various types of graphitic carbons, including graphene oxide, specifically with the aim to identify the type of defects.

Herein, we applied the XPDF to the characterisation of solution-processed graphene produced by LPE and EC and dispersed in different solvents. The geometrical arrangement of carbon atoms in the ring has been obtained from the analysis of the XPDF data. We observe structural deformations of the hexagonal carbon ring, compared to the perfect planar geometry, inducing possible rippling at the scale of the inter-atomic distances, which could be related to the interaction with the solvent molecules, as predicted theoretically.

2. Results and discussion

Solution-processed graphene was produced by using cathodic EC and LPE methods, as outlined in figures 1(A) and (B), (and supplementary figure S1(a)) following the approaches reported previously [12, 29–31]. The solution process graphene in either NMP and Cy are named as Gr LPE (NMP) Gr LPE (Cy), Gr EC (NMP) and Gr EC (Cy), respectively. The chemical structure of Cy is shown supplementary figure S1(b). The measurements were performed directly in solution. In the case of EC graphene, the expanded graphite powder (EC powder) was also collected and measured in solid form. Commercially available graphite was also measured as a reference. The graphene concentration is determined by UV–vis spectroscopy using an absorption coefficient of $2207 \, \mathrm{l \, g^{-1} \, m^{-1}}$ [32] and $2460 \, \mathrm{l \, g^{-1} \, m^{-1}}$ [11] for EC and LPE graphene, respectively, measured at 660 nm. The concentrations are reported in table S1, in the supplementary information.

The graphene nanosheets have been characterised by atomic force microscopy (AFM), Raman spectroscopy, high resolution transmission electron microscopy (HRTEM) and x-ray photoelectron spectroscopy (XPS). The thickness and lateral size distributions of both LPE and EC graphene flakes were estimated by AFM (figures 2(A) and (D)). Figures 2(B) and (E) show the statistics of the peak thickness of the LPE and EC graphene, respectively, as extracted from AFM measurements, done over 300 individual flakes, revealing that the dispersions are mostly composed of thin (<10 layers) graphene flakes. The lateral size distribution of LPE and EC graphene in figures 2(C) and (F), respectively, shows

Figure 2. (A) Typical AFM image of LPE graphene drop-casted on SiO₂/Si substrate; (B) thickness and (C) lateral size distribution of LPE graphene measured by AFM; (D) typical AFM image of EC graphene; (E) number of layers and (F) lateral size distribution of EC graphene measured by AFM; (G) and (H) representative Raman spectra of LPE and EG graphene measured with 514.5 nm laser, respectively; (I) HRTEM images of LPE graphene, inset shows the corresponding FFT image; (J) TEM image of the EC graphene, inset is the SAED pattern; (K) and (L) XPS C 1s spectra of LPE and EC graphene, respectively.

that the as-prepared graphene nanosheets follows a broad distribution in size, where the average lateral size for the LPE Gr was ∼223 nm and between 1 and 4 μm for the EC Gr. The smaller flake size for the LPE Gr compared to the EC Gr is due to the extensive sonication during the exfoliation process and is in good agreement with our previous reports [7, 12]. Figures 2(G) and (H) shows representative Raman spectra measured on individual flakes produced by

LPE and EC, respectively. The typical Raman spectrum of LPE and EC Gr shows the D and G peaks at ∼1350 cm^{-1} and ∼1580 cm^{-1}, respectively [33]. The D peak is activated by defects, but the specific activation mechanism is different between the two samples. In the case of graphene produced by LPE, the D peak is activated by the edges of the nanosheets, having lateral size comparable or smaller than that of the laser spot size [34]. The D peak in the Raman

spectrum of EC graphene (figure 2(H)) is likely activated by introducing functional groups during the electrochemical treatment, as evidenced by the XPS results. It should also be noted that the gas bubbles collapse on the electrodes could form different kinds of defects in the graphene basal plane, including generating some vacancies. These defects could also be a result of structural defects introduced by the gas evolution between the layers caused by the repeated ion intercalation/deintercalation process during the exfoliation process.

High resolution TEM (HRTEM) images reveal that the graphene nanosheets produced by the LPE and EC processes are clean and of high crystallinity. Moreover, both the FFT and SAED patterns of LPE and EC graphene (inset of figures 2(I) and (J), respectively) reveal the bright inner ring of {0–110} spots and faint outer ring of {1–210} spots, in agreement with the typical diffraction pattern of monolayer graphene. Moreover, the High-Angle Annular Dark Field (HAADF) and the corresponding energy disperse spectroscopy (EDS) mapping of the graphene flake (supplementary figure S2) demonstrate that graphene produced by the LPE process consists of pristine flakes without any impurities.

The chemical composition of the as-prepared graphene was further investigated by the XPS. As shown in figures 2(J) and (K), both the XPS spectra of the LPE and EC graphene show asymmetric C 1s peak centred ~284 eV corresponding to sp^2 C–C bond. Noticeably, only a tiny amount of oxygen related functional groups (i.e. C–OH and C=O groups at 285.5 eV and 288.4 eV, respectively) were observed in LPE Gr, which mainly inherited form the starting graphite used for the exfoliation process [35]. On the other hand, the oxygen content of the EC Gr was found to be around 7.8 at% compared to the 5.5 at% of pure graphite (supplementary figures S3 and S4), supporting the assumption the EC exfoliation process used is largely nonoxidative. Therefore, both the LPE and EC Gr used in this study are of high quality and crystallinity as supported by different characterization methods discussed above.
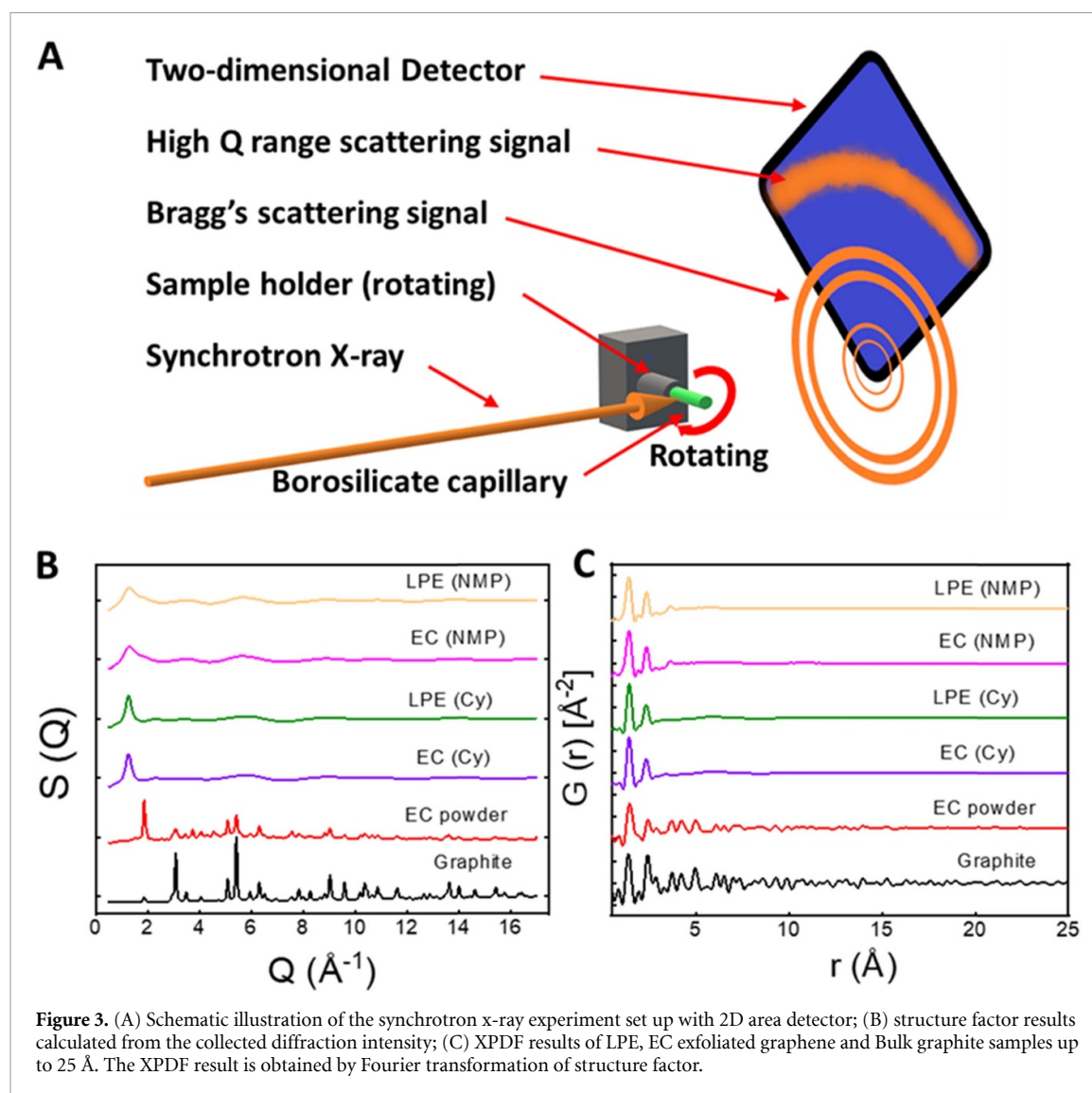
For x-ray characterization, the samples were packed in a borosilicate capillary with 1.5 mm diameter. The background signal measurement is conducted, (as shown in supplementary figure S5) and subtracted from the signal of the graphene. As shown in figure 3(A), during the synchrotron x-ray experiments, the capillaries are mounted horizontally and rotate about its long axis centring the x-ray beam at the upper half of the capillary to avoid any precipitations of the highly concentrated solution sample. The exposure time for each x-ray scattering measurement was 300 s. The experimentally collected diffraction intensity data, including Bragg's scattering signal and high Q range scattering signal can be primarily processed into the total scattering structure function, $S(Q)$, representing the normalised scattering cross-section form [21]. A highly monochromatic synchrotron x-ray beam was used; hence zero bremsstrahlung contribution can be assumed. The top-hat width for the Lorch function of 1.0 Å^{-1} was utilised, and a minimum Fourier filter radius of 1.25 Å^{-1} was used for the Fourier transform.

Figure 3(B) shows the $S(Q)$ of all the samples after subtraction of the background. In the case of graphite, the intense peak-like features are characteristic of a three-dimensional and highly crystalline structure. In the case of EC powder, the peaks over $Q = 3 \text{ Å}^{-1}$ decrease in intensity, while the intensity of the peak just below $Q = 2 \text{ Å}^{-1}$ increases. The solution-processed graphene obtained by LPE and by cathodic EC show a similar spectrum, characterised by a broad peak at about $Q = 1.1 \text{ Å}^{-1}$. The missing/decreased intensity of the peaks is related to a change in structure, associated with a reduced ordered configuration of the atoms. The processed XPDF spectra up to 25 Å is shown in figure 3(C). Graphite shows obvious atomic correlations up to 15 Å or more. In the case of the graphite powder, the correlation is visible up to 10 Å. On the other hand, in the case of solution-processed graphene, long-distance correlations are completely missing. The absence of long-distance correlation peaks indicates the disappearance of the three-dimensional (3D) structure due to the exfoliation (as in the case of LPE and EC samples). The exfoliation caused lack of repeated atomic correlation between the layers of graphite (i.e. loss of AB-stacking), as in the case of the EC powder.

In the case of solution-processed graphene, only the two peaks at short correlation distances (<5 Å) are clearly visible. However, a closer look in this region, figure 4(A), shows that the number of peaks and their positions is slightly different, depending on the sample considered. These peaks are very important because their position is associated with the C–C atomic distance in the ring: by using the carbon hexagon model from graphite in figure 4(B), one would expect to see five peaks at the distances 1.41 Å, 2.42 Å, 2.86 Å, 3.74 Å, 4.22 Å, corresponding to the C1–C2, C1–C3, CI–C4, C1–C5, C1–C6 atomic distances, respectively. This is well observed with the selected Q range of XPDF spectrum, as shown in figure 4(A), which also agrees with previous research [36, 37].

Figure 4(C) shows that the C1–C2 bonding in graphite powder increases up to 1.46 Å, while it is fixed at 1.43 Å or 1.44 Å for solution-processed graphene, irrespective of the exfoliation method used. Note that cathodic graphene has a size comparable to graphene flakes made by LPE [12]. The C1–C3 distance slightly increases in graphite powder compared to bulk graphite, while it is much smaller in the case of solution-processed graphene. The same is observed for C1–C4, although the signal of solution-processed

Figure 3. (A) Schematic illustration of the synchrotron x-ray experiment set up with 2D area detector; (B) structure factor results calculated from the collected diffraction intensity; (C) XPDF results of LPE, EC exfoliated graphene and Bulk graphite samples up to 25 Å. The XPDF result is obtained by Fourier transformation of structure factor.
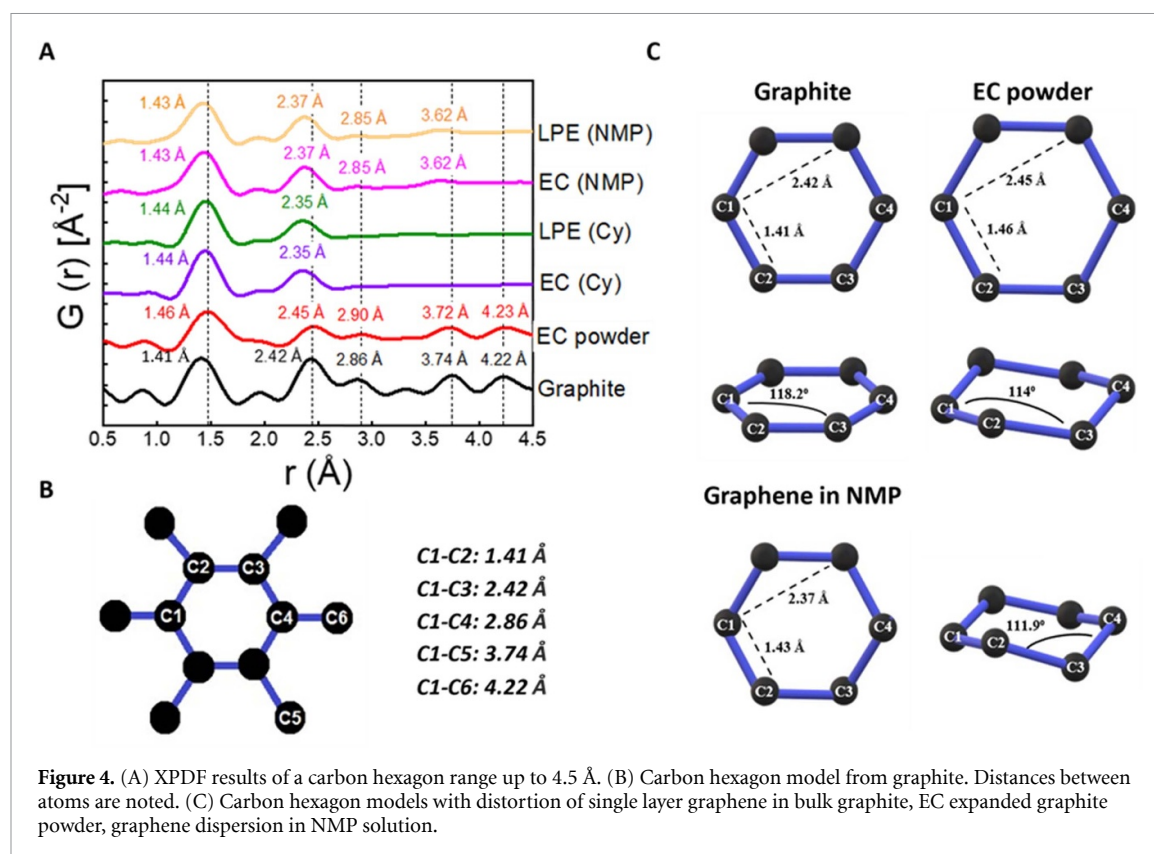
graphene is rather weak with a broad peak but can still be recognised at about 2.85 Å, which indicates that the C1–C4 atomic correlation is hardly visible measured as a fixed value. In the case of the C1–C5 distance, no significant differences are observed between bulk graphite and EC graphite powder. In contrast, the C1–C5 distances are reduced in the case of solution-processed graphene, with no dependence on the exfoliation method. The peak associated with C1–C6 is missing in the case of solution-processed graphene. The correlation of longer distance C1–C6 becomes too weak to be detected by the XPDF, which can be regarded as uncorrelated pair.

Interestingly, any correlation associated with NMP or Cyrene (for structure details readers are referred to [29]) is not observed in solution-processed graphene. The intermolecular correlation of the solvent molecules could be visible if the molecules are ordered in space. However, the NMP and Cyrene molecules are probably randomly spaced with relatively low concentration, which

means no constructive scattering can occur even without removing the background. Therefore, all of the characteristic peaks of the solvent molecules are not observed in our spectra. All the correlation peaks, and in particular the one at 1.43–1.44 Å for solution-processed graphene, are doubtlessly coming from graphene. Thus, the difference between graphene in NMP and Cyrene is minimal and can be neglected [29].

The XPDF results confirm that cathodic EC and LPE can provide nanosheets with thickness small enough to be considered two-dimensional. However, slightly different geometric arrangements of the atoms in the hexagonal ring have been observed as compared to graphite. Figure 4(C) shows the resulting carbon hexagon models for solution-processed graphene in NMP and EC graphite powder compared to that of graphite. Our results show that ion intercalation and related layers' expansion, caused by the cathodic EC process, gives rise to a small ring distortion compared to pristine graphene. However, the

Figure 4. (A) XPDF results of a carbon hexagon range up to 4.5 Å. (B) Carbon hexagon model from graphite. Distances between atoms are noted. (C) Carbon hexagon models with distortion of single layer graphene in bulk graphite, EC expanded graphite powder, graphene dispersion in NMP solution.

ring distortion further increases when the material is dispersed in a solvent. Remarkably, as both LPE and EC graphene dispersed in the same solvent show exactly the same type of distortion of the hexagonal ring, this effect is likely to be caused by the interaction between solvent molecules and graphene. Nevertheless, further research needs to done to fully confirm this observation.

Meyer *et al* [38] have suggested ripples in suspended graphene through TEM investigations, as confirmed by other groups [39–41]. In particular, an average of 0.7 Å height fluctuation (i.e. ripple height normal to the sheet) was found by using Monte Carlo simulation [42]. The bond length deviation is predicted from 1.31 Å to 1.54 Å. This could include the short double bond of 1.31 Å, a conjugated bond of 1.42 Å, and up to a long single bond of 1.54 Å. Hence, the three bonds of each carbon atom within the hexagon could be different. Our results show ring distortions compatible with the proposed model for suspended graphene [39]; as the C1–C3 atomic distance of solution-processed graphene becomes shorter than the bulk graphite. However, it needs to be noted that TEM measurements were done on the suspended graphene while our measurements were obtained for graphene in solution. The increasing bond lengths differences indicate that the graphene's increased density is not perfectly planar when dispersed in a solvent. The bonding angle between C1–C2–C3 is

calculated as 111.9° and 114° for graphene dispersion and powder. The normal surface angle to the sheet of the powder sample should be less than 6° (i.e. the angle deviation of 114° from 120°), in agreement with the angle deviation from Meyer's work [38], where the angle deviation from the sheet is ±5°. Likely, this effect is caused by the interaction of the solvent with graphene.

3. Conclusions

Our work presents the first characterisation of solution-processed graphene in NMP and Cyrene by high energy x-ray scattering and related XPDF analysis. The results show the disappearance of long-range atomic correlations, confirming the production of 2D nanosheets and that the hexagonal atomic structure is strongly distorted when graphene is suspended in a medium. In particular, the first C–C distance slightly increases, while the second C–C distance decreases, resulting in a distortion that could be compatible with ripples formation observed in suspended graphene, likely to be caused by the interaction of solvent molecules with the graphene nanosheets. Our results demonstrate the potential of XPDF as a powerful tool to characterise 2D materials and acquire quantitative structural information with atomic resolution.

4. Methods

4.1. Materials
High purity graphite foil (99.8% metal basis), graphite rod (99.99% metal basis) and ammonium sulfate $((NH_4)_2SO_4, 98+\%)$ were purchased from Alfa Aesar. Anhydrous dimethyl sulfoxide (DMSO) (99.9%), graphite flakes (100+ mesh), 1-Pyrenesulfonic acid sodium salt (PS1) and iso-propyl alcohol (IPA) were purchased from Sigma-Aldrich. Isomolded graphite (>99.95%) rods were purchased from GraphiteStore. Cesium perchlorate (99%) was obtained from Fisher Scientific. The natural kish graphite was bought from Graphexel Ltd. All the chemicals and materials were used as received.

4.2. Exfoliation
The LPE graphene in NMP was prepared by adding 300 mg of graphite flakes into 100 ml of NMP, followed by sonicating the mixture at 600 W using Hilsonic bath sonicator for 5 d. Afterwards, the dispersion was centrifuged using a Sigma 1–14k refrigerated centrifuge at 903 g for 20 min to remove un-exfoliated graphite. To obtain highly concentrated graphene, the dispersion was further centrifuged at 16 600 g for 1 h., followed by re-dispersing the sedimented graphene into a small volume of NMP. The EC is prepared by the cathodic electrochemical exfoliation as described in our previous work [12]. Briefly, a pellet of natural graphite is used as a cathode, and Pt mesh was used as the anode. The electrolyte was 1M lithium chloride (Sigma Aldrich, 99.9%), and Triethylamine hydrochloride in dimethyl sulfoxide. The exfoliation products were washed to remove the electrolyte with water and ethanol until the pH was neutral, and the products were separated by filtration using Anodisc alumina membranes with 100 nm pore size and then dried at 200 °C under Ar atmosphere. The dry powder was then dispersed in a small amount of NMA, as in the LPE samples.

4.3. Materials characterization
UV–Vis spectroscopy of the graphene dispersions were measured by using a PerkinElmer I-900 UV–Vis–NIR spectrometer. A Bruker Atomic Froce Microscope (MultiMode 8) in Peak Force Tapping mode, equipped with ScanAsyst-Air tips is used to determine the lateral size and thickness distribution of the graphene flakes. The samples were prepared by drop casting the dispersion on a clean silicon substrate; several hundreds of individual flakes were selected, after complete solvent evaporation, for lateral size and thickness analysis. The same sample preparation has been used for Raman measurements. Raman measurements were performed using a Renishaw Invia Raman spectrometer equipped with a 514.5 nm excitation line with 1 mW laser power. 100× NA0.85 objective lens, giving a spatial resolution of ∼500 nm, and 2400 grooves nm^{-1} grating

were used for the measurements. The x-ray photoelectron spectroscopy (XPS) measurements were performed using the K-Alpha x-ray Photoelectron Spectrometer (XPS) System from Thermo Scientific. The photon source was a monochromatized Al Kα line ($h\nu = 1486.6$ eV). The spectra were acquired using a spot size of 300 μm and constant pass energy (150 eV for survey and 20 eV for high resolution spectra). A flood gun with combined electrons and low energy Ar ions is used during the measurements. HRTEM images were acquired on a JEOL 2100-F microscope with a field-emission gun operated at 200 kV accelerating voltage providing direct images of the atomic structure. A HAADF detector and an Oxford high solid-angle silicon drift detector x-ray energy dispersive spectrometer (EDS) system was used for chemical elemental analysis.

4.4. X-ray scattering
The synchrotron x-ray scattering experiments were conducted in I15–1 beamline, Diamond Light Source, U.K. The monochromatic x-ray beam with 76.7 keV (wavelength of 0.161 669 Å) was employed [43]. A 2D Perkin Elmer XRD detector with active area of 409.6 × 409.6 mm^2, and pixel size of 100 μm was applied close to sample to provide large Q range and high-quality scattering data. Here $Q = (4\pi \sin\theta)/\lambda$, where λ is the wavelength and 2θ is the angle between incident and scattered x-rays. The collected diffraction intensity data is processed by software GudrunX [44] which subtracts the self-scattering intensity, Compton scattering and multiple scattering, etc. Then, the total scattering structure factor, *S(Q)* and XPDF, *G(r)* are obtained as;

$$S(Q) = \frac{I(Q)}{b^2} \tag{1}$$

$$G(r) = \frac{2}{\pi} \int_{Q_{min}}^{Q_{max}} Q[S(Q) - 1]\sin(Qr)\,dQ \tag{2}$$

where *I(Q)* is the collected and processed diffraction intensity. The coherent single-scattering intensity is desired; *b* is the element scattering amplitude (*f* is used for x-ray scattering); <…> denotes an averaging process. For detailed theory, [21, 45] is referred.

Author contributions

Z Y, A A and W M conceived the approach and designed the experiments. A A, W M, and TF carried out the x-ray experiments while M G and K P prepared materials and carried out lab experiments. O R, C D and J U performed the material characterizations with AFM, HRTEM, EDS and XPS analysis. Z Y performed the analysis the data and drafted the manuscript with inputs from C C, A A and W M. All authors discussed the results and contributed to the manuscript.

ORCID iDs

Zhengyu Yan ⬤ https://orcid.org/0000-0002-2543-8207
María J G Guimarey ⬤ https://orcid.org/0000-0003-0483-4136
Khaled Parvez ⬤ https://orcid.org/0000-0003-2851-9907
Chaochao Dun ⬤ https://orcid.org/0000-0002-3215-6478
Oliver Read ⬤ https://orcid.org/0000-0001-9771-6096
Jeffrey J Urban ⬤ https://orcid.org/0000-0003-4909-2869
Cinzia Casiraghi ⬤ https://orcid.org/0000-0001-7185-0377
Wajira Mirihanage ⬤ https://orcid.org/0000-0002-9083-269X

References

[1] Bonaccorso F, Bartolotta A, Coleman J N and Backes C 2016 2D-crystal-based functional inks *Adv. Mater.* **28** 6136–66

[2] Backes C *et al* 2020 Production and processing of graphene and related materials *2D Mater.* **7** 022001

[3] Cai X, Luo Y, Liu B and Cheng H-M 2018 Preparation of 2D material dispersions and their applications *Chem. Soc. Rev.* **47** 6224–66

[4] Ciesielski A and Samorì P 2014 Graphene via sonication assisted liquid-phase exfoliation *Chem. Soc. Rev.* **43** 381–98

[5] Kelly A G *et al* 2017 All-printed thin-film transistors from networks of liquid-exfoliated nanosheets *Science* **356** 69–73

[6] Secor E B and Hersam M C 2015 Emerging carbon and post-carbon nanomaterial inks for printed electronics *J. Phys. Chem. Lett.* **6** 620–6

[7] McManus D *et al* 2017 Water-based and biocompatible 2D crystal inks for all-inkjet-printed heterostructures *Nat. Nanotechnol.* **12** 343–50

[8] Torrisi F *et al* 2012 Inkjet-printed graphene electronics *ACS Nano* **6** 2992–3006

[9] Nicolosi V, Chhowalla M, Kanatzidis M G, Strano M S and Coleman J N 2013 Liquid exfoliation of layered materials *Science* **340** 1226419

[10] Backes C, Higgins T M, Kelly A, Boland C, Harvey A, Hanlon D and Coleman J N 2017 Guidelines for exfoliation, characterization and processing of layered materials produced by liquid exfoliation *Chem. Mater.* **29** 243–55

[11] Hernandez Y *et al* 2008 High-yield production of graphene by liquid-phase exfoliation of graphite *Nat. Nanotechnol.* **3** 563–8

[12] Abdelkader A M, Kinloch I A and Dryfe R A W 2014 Continuous electrochemical exfoliation of micrometer-sized graphene using synergistic ion intercalations and organic solvents *ACS Appl. Mater. Interfaces* **6** 1632–9

[13] Abdelkader A M 2015 Electrochemical synthesis of highly corrugated graphene sheets for high performance supercapacitors *J. Mater. Chem.* A **3** 8519–25

[14] Parvez K, Wu Z-S, Li R, Liu X, Graf R, Feng X and Müllen K 2014 Exfoliation of graphite into graphene in aqueous solutions of inorganic salts *J. Am. Chem. Soc.* **136** 6083–91

[15] Cooper A J, Wilson N R, Kinloch I A and Dryfe R A W 2014 Single stage electrochemical exfoliation method for the production of few-layer graphene via intercalation of tetraalkylammonium cations *Carbon* **66** 340–50

[16] Yang Y, Lu F, Zhou Z, Song W, Chen Q and Ji X 2013 Electrochemically cathodic exfoliation of graphene sheets in room temperature ionic liquids N-butyl, methylpyrrolidinium bis(trifluoromethylsulfonyl)imide and their electrochemical properties *Electrochim. Acta* **113** 9–16

[17] Wick P *et al* 2014 Classification framework for graphene-based materials *Angew. Chem. Int. Ed.* **53** 7714–8

[18] Kostarelos K and Novoselov K S 2014 Graphene devices for life *Nat. Nanotechnol.* **9** 744–5

[19] Pollard A J *et al* 2017 Characterisation of the structure of graphene (available at: https://eprintspublications.npl.co.uk/8654/)

[20] ISO/TS 21356–1 2021 *Nanotechnologies—Structural Characterization of Graphene—Part 1: Graphene from Powders and Dispersions* (International Organisation for Standardization) (available at www.iso.org/standard/70757.html)

[21] Egami T and Billinge S J L Eds 2012 *Underneath the Bragg Peaks Structural Analysis of Complex Materials* vol 16 (Oxford: Pergamon)

[22] Bilderback D H, Elleaume P and Weckert E 2005 Review of third and next generation synchrotron light sources *J. Phys. B: At. Mol. Opt. Phys.* **38** S773–97

[23] Hastings J B, Thomlinson W and Cox D E 1984 Synchrotron x-ray powder diffraction *J. Appl. Crystallogr.* **17** 85–95

[24] Westneat M W, Socha J J and Lee W-K 2008 Advances in biological structure, function, and physiology using synchrotron x-ray imaging *Annu. Rev. Physiol.* **70** 119–42

[25] Smith M A, Foley H C and Lobo R F 2004 A simple model describes the PDF of a non-graphitising carbon *Carbon* **42** 2041–8

[26] Petkov V, Difrancesco R G, Billinge S J L, Acharya M and Foley H C 1999 Local structure of nanoporous carbons *Phil. Mag.* B **79** 1519–30

[27] Woznica N, Hawelek L, Fischer H E, Bobrinetskiy I and Burian A 2015 The atomic scale structure of graphene powder studied by neutron and x-ray diffraction *J. Appl. Crystallogr.* **48** 1429–36

[28] Woźnica N, Hawelek L, Duber S, Fischer H E, Honkimäki V, Pawlyta M, Bulou A and Burian A 2017 The atomic scale structure of saccharose-based carbons *Phil. Mag.* **97** 1675–97

[29] Salavagione H J, Sherwood J, De Bruyn M, Budarin V L, Ellis G J, Clark J H and Shuttleworth P S 2017 Identification of high performance solvents for the sustainable processing of graphene *Green Chem.* **19** 2550–60

[30] Coleman J N 2013 Liquid exfoliation of defect-free graphene *Acc. Chem. Res.* **46** 14–22

[31] Wang J, Manga K K, Bao Q and Loh K P 2011 High-yield synthesis of few-layer graphene flakes through electrochemical expansion of graphite in propylene carbonate electrolyte *J. Am. Chem. Soc.* **133** 8888–91

[32] Parvez K, Worsley R, Alieva A, Felten A and Casiraghi C 2019 Water-based and inkjet printable inks made by electrochemically exfoliated graphene *Carbon* **149** 213–21

[33] Nagyte V *et al* 2020 Raman fingerprints of graphene produced by anodic electrochemical exfoliation *Nano Lett.* **20** 3411–9

[34] Casiraghi C, Hartschuh A, Qian H, Piscanec S, Georgi C, Fasoli A, Novoselov K S, Basko D M and Ferrari A C 2009 Raman spectroscopy of graphene edges *Nano Lett.* **9** 1433–41

[35] Shang N G, Papakonstantinou P, Sharma S, Lubarsky G, Li M, McNeill D W, Quinn A J, Zhou W and Blackley R 2012 Controllable selective exfoliation of high-quality graphene nanosheets and nanodots by ionic liquid assisted grinding *Chem. Commun.* **48** 1877

[36] Petkov V, Ren Y, Kabekkodu S and Murphy D 2013 Atomic pair distribution functions analysis of disordered low-Z materials *Phys. Chem. Chem. Phys.* **15** 8544

[37] Burian A, Dore J C and Jurkiewicz K 2019 Structural studies of carbons by neutron and x-ray scattering *Rep. Prog. Phys.* **82** 016501

[38] Meyer J C, Geim A K, Katsnelson M I, Novoselov K S, Booth T J and Roth S 2007 The structure of suspended graphene sheets *Nature* **446** 60–63

[39] Amiri A, Naraghi M, Ahmadi G, Soleymaniha M and Shanbedi M 2018 A review on liquid-phase exfoliation for scalable production of pure graphene, wrinkled, crumpled and functionalized graphene and challenges *FlatChem* **8** 40–71

[40] Li Z, Kinloch I A, Young R J, Novoselov K S, Anagnostopoulos G, Parthenios J, Galiotis C, Papagelis K, Lu C-Y and Britnell L 2015 Deformation of wrinkled graphene *ACS Nano* **9** 3917–25

[41] Liu N, Pan Z, Fu L, Zhang C, Dai B and Liu Z 2011 The origin of wrinkles on transferred graphene *Nano Res.* **4** 996–1004

[42] Fasolino A, Los J H and Katsnelson M I 2007 Intrinsic ripples in graphene *Nat. Mater.* **6** 858–61

[43] Chater P A, Keeble D, Wharmby M, Spain T, Filik J and Wilhelm H 2017 The automated XPDF beamline at diamond light source *Acta Crystallogr.* A **73** C69

[44] Keen D A 2001 A comparison of various commonly used correlation functions for describing total scattering *J. Appl. Crystallogr.* **34** 172–7

[45] Billinge S J L 2019 The rise of the x-ray atomic pair distribution function method: a series of fortunate events *Phil. Trans. R. Soc.* A **377** 20180413